Position-dependent property of resonant dipole–dipole interaction mediated by localized surface plasmon of an Ag nanosphere*

Xu Dan(许 丹), Wang Xiao-Yun(王小云)†, Huang Yong-Gang(黄勇刚), Ouyang Shi-Liang(欧阳仕粮), He Hai-Long(何海龙), and He Hao(何 浩)

College of Physics, Mechanical and Electrical Engineering, Jishou University, Jishou 416000, *China*

(Received 22 May 2014; revised manuscript received 2 September 2014; published online 10 December 2014)

We use the photon Green-function method to study the quantum resonant dipole–dipole interaction (RDDI) induced by an Ag nanosphere (ANP). As the distance between the two dipoles increases, the RDDI becomes weaker, which is accompanied by the influence of the higher-order mode of the ANP on RDDI declining more quickly than that of the dipole mode. Across a broad frequency range (above 0.05 eV), the transfer rate of the RDDI is nearly constant since the two dipoles are fixed at the proper position. In addition, this phenomenon still exists for slightly different radius of the ANPs. We find that the frequency corresponding to the maximum transfer rate of RDDI exhibits a monotonic decrease by moving away one dipole as the other dipole and the ANP are kept fixed. In addition, the radius of ANP has little effect on this. When the two dipoles are far from the ANP, the maximum transfer rate of the RDDI takes place at the frequency of the dipole mode. In contrast, when the two dipoles are close to the ANP, the higher-order modes come into effect and they will play a leading role in the RDDI if they match the transition frequency of the dipole. Our results may be used in a biological detector and have a certain guiding significance for further application.

Keywords: quantum resonant dipole–dipole interaction, photonic Green function, surface plasmon

PACS: 42.50.Ct, 34.20.–b, 73.20.Mf **DOI:** 10.1088/1674-1056/24/2/024205

1. Introduction

The effect of an electromagnetic field on the radiation property has been completely investigated and sorted into quantum electrodynamics (QED), which is based on the prediction that the spontaneous emission rate could be tailored by using the electromagnetic environment that was developed by Purcell.[1] The characteristics of QED have been studied in both theory and experiment, and a variety of QED devices have been proposed and developed by many researchers.[2–8] Some novel concepts, such as enhanced and inhibited spontaneous emission,[5,8] reversible spontaneous emission,[6] and the one-atom maser,[9] have been well known.

The quantum RDDI can be highly modulated by the electromagnetic environment. Two two-level atoms, one is excited and the other stays in the ground state, can interact with each other by exchanging a photon. A photon emitted by the excited atom can be absorbed by the other atom in the ground state. The transfer rate of the RDDI and the RDDI potential energy is determined by the rates of photon emission, transmission and absorption. A variety of electromagnetic environments have been used to control and modify these characteristics, such as a vacuum,[8,10] optical cavities,[11,12] photonic materials,[13] and metal surfaces,[14,15] and so on. For example, a metal surface can concentrate light into a nanoscale spatial region near the metal/dielectric interface by the excitation of surface plasmons (SPs). This ability can extremely enhance the rates of photon emission and absorption. In particular, by rationally designing and optimizing geometry, the metallic structures can be beneficial to collecting the emitted photons from one dipole and transferring them to the other dipole efficiently.

Metal nanosphere (MNP) is a promising platform to investigate the quantum RDDI, where they induce the localized surface plasmon resonances (LSPRs) under light illumination. A surface plasmon polariton (SPP)-based waveguide is a potential candidate for guiding light due to its ability to achieve the nanoscale confinement of an incident optical field in two dimensions. As a result, it has been regarded as a building block for the novel ultracompact photonic device and integrated circuit.[16] Up to now, large numbers of SPP-based waveguiding structures have been investigated, including hybrid plasmonic waveguides,[17] metal stripes embedded in homogeneous dielectrics,[18] metallic nanowires,[19] metal slots,[20] etc. However, SPP-based waveguides can only confine light in two dimensions. In contrast, LSPRs from an MNP can concentrate the optical energy in three dimensions and thus find a wide application prospect in integrated plasmonic circuits, for instance, an LSPR-based sensor, an SP-based photoswitch, and an SP-based laser.[21] All these applications benefit from the extremely amplified and tightly confined local field, which leads to an ultra-small mode volume that signifi-

*Project supported by the National Natural Science Foundation of China (Grant Nos. 11347215, 11464014, and 11104113), the Natural Science Foundation of Hunan Province, China (Grant Nos. 13JJ6059 and 13JJB015), and the Natural Science Foundation of Education Department of Hunan Province, China (Grant Nos. 13C750 and 13B091).

†Corresponding author. E-mail: wxyyun@163.com

© 2015 Chinese Physical Society and IOP Publishing Ltd

cantly increases the light-matter interaction. Based on this unparalleled ability, the MNP is expected to remarkably improve the photon emission and absorption rates of the two nearby dipoles, as well as the RDDI between them.

Recent studies show that this kind of interaction has been applied to implement quantum entanglement preparation and quantum information processing,[15,22–28] cooperative radiation,[29] Förster energy transfer,[30,31] dipole nanolasers,[32] etc. Furthermore, some novel quantum phenomena have been found.[33–35] All of these applications and phenomena mentioned above are related in essence to the transfer rate or RDDI potential energy.

In previous theoretical studies, the transfer rate and the RDDI potential energy are obtained by numerical methods[15,24,35–38] or analytic methods.[39–43] For numerical methods, an independent program needs to sweep the parameters for the dipoles at different positions or with different polarizations, where a single run usually needs considerable computational resources for the finite element method (FEM) or the finite-difference time-domain (FDTD) method. However, for a relatively simple electromagnetic environment, such as the structure of an ANP, we can treat the problem by using the analytical Green function.[44]

The Green function $G(\boldsymbol{r},\boldsymbol{r}';\omega)$ describes the propagation of photons from the source point $(\boldsymbol{r}')$ to the point $(\boldsymbol{r})$ with an angular frequency (ω). It includes all of the possible scattering events and the information about the probability that a photon will arrive at a particular location for a given excitation source. The transfer rate and the RDDI potential energy can be expressed by the Green function. Here, we adopt the analytical Green function approach to investigate the quantum RDDI mediated that is by the LSPR of an ANP.

In this work, we systematically analyze the quantum RDDI induced by an ANP. Firstly, we examine the effect of the ANP on the spontaneous emission rate which determines the strength of the corresponding transfer rate. We find that as the distance between the quantum dot (QD) and the surface of the ANP is increased, the spontaneous emission rate decreases and the effect of ANP higher-order mode dominates compared with that of the dipole mode. We then further study the effect of the distance between the two QDs on the transfer rate of the RDDI by fixing one QD at x axis and change the position of the other one along x axis, here we consider the two QDs that are on the same side of the ANP. We find that the transfer rate of the RDDI nearly keeps constant in a broad frequency range for a set of ANPs with a slightly different radius. In addition, the frequency corresponding to the maximum of transfer rate of RDDI shows a monotonic decrease as the distance between QD and ANP is increased. Finally, we consider two general cases where one QD is fixed far from or nearly touches the surface of the ANP. We investigate the property of the transfer rate by changing the location of the other QD on the same plane. It is shown that the dipole mode of the ANP makes a main contribution to the transfer rate of RDDI when the QDs are far from the ANP. While the QDs are close to ANP, the higher-order modes may be the major factors depending on the transition frequency of the dipole.

2. Model and solution

A schematic diagram of the system is illustrated in Fig. 1. An ANP with radius a is located at the origin. QD (A) is located at the x axis with a distance of $d_{\rm a}$ from the surface of ANP, and u_i is its transition dipole moment. QD (B) is fixed on a line with the angle φ included between the line and x axis, its distance is $d_{\rm b}$ from the surface of the ANP and u_j is its transition dipole moment.

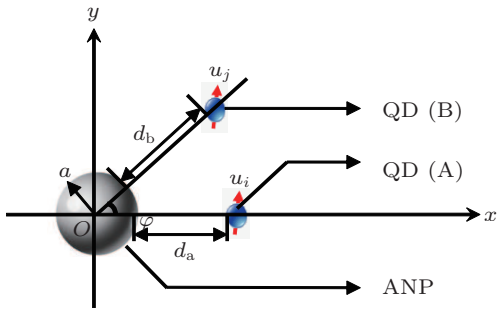


Fig. 1. (color online) Schematic diagram of the system for the coupled QD-ANP system.

According to Refs. [31] and [44], the transfer rate and the potential energy of the RDDI in the quantization scheme are

$$\delta_{ij}=\frac{1}{\hbar\varepsilon_0}\,\mathrm{Re}\,u_i\cdot G(r_i,r_j,\omega)\cdot u_j, \tag{1}$$

$$\Gamma_{ij}=\frac{2}{\hbar\varepsilon_0}\,\mathrm{Im}\,u_i\cdot G(r_i,r_j,\omega)\cdot u_j, \tag{2}$$

where i and j represent QD (A) and QD (B), respectively, Γ_{ij} and δ_{ij} are the transfer rate and potential energy of the RDDI, respectively, r_i and r_j refer to their spatial positions, ω refers to the transition frequency, ε_0 is the vacuum permittivity, $\hbar$ is the Planck constant, and $G(\boldsymbol{r}_i,\boldsymbol{r}_j,\omega)$ is the Green tensor. The Green function in a medium with $\varepsilon(\boldsymbol{r},\omega)$ (complex dielectric constant) and $\mu=1$ is given as[45,46]

$$\nabla\times\nabla\times G(\boldsymbol{r},\boldsymbol{r}';\omega)-\varepsilon(\boldsymbol{r},\omega)k_0^2G(\boldsymbol{r},\boldsymbol{r}';\omega)=k_0^2\delta(\boldsymbol{r}-\boldsymbol{r}'),$$

where $k_0=\omega/c$, ω is the angular frequency and c refers to the speed of light.

For these calculations, we use an established analytical approach where the Green function is expanded in spherical vector functions.[43,46] The specific expressions are given in Appendix A.

3. Discussion

On the basis of the above results, we can analyze the transfer rate (Γ_{ij}) and potential energy (δ_{ij}) of the quantum RDDI. QDs A and B are located at the x axis with the distances of d_a and d_b from the surface of ANP, respectively, the transition dipole moment u_i is equal to u_j and radius of ANP is a. According to Refs. [25] and [26], we can easily obtain $\Gamma_{ij} \leq \sqrt{\Gamma_{ii}\Gamma_{jj}}$ (Γ_{ii} and Γ_{jj} are the spontaneous emission rate). We first investigate the effect of the ANP on Γ_{ii} which determines the maximum strength of Γ_{ij}. Here, we set $a = 20$ nm and study the effect of distance d between the QD and the surface of the ANP on Γ_{ii}.

The normalized spontaneous emission rate (Γ_{ii}/Γ_0) is shown in Figs. 2(a) and 2(b) corresponding to the small and large d, respectively. $\Gamma_0(\omega) = u^2\omega^3/3\pi\varepsilon_0\hbar c^3$, where Γ_0 is the local coupling strength for a two-level atom at transition frequency ω of the bare atom in vacuum and u is the transition dipole moment. From Fig. 2(a) it follows that Γ_{ii} exhibits three main peaks. As explained by Hughes,[24] the peak of Γ_{ii} at the lowest frequency is caused mainly by the dipole mode while the other peaks at higher frequencies arise from the higher-order modes. As d is increased, Γ_{ii} becomes weak and the peak of the ANP's dipole modes on Γ_{ii} decreases more slowly than that of the higher-order modes. For example, when $d = 2$ nm, the values of Γ_{ii} are above 1.9×10^5 and 7.5×10^3 at the frequencies of the ANP's higher-order mode and dipole mode, respectively. While $d = 6$ nm, the values of Γ_{ii} decrease to 4600 and 1300 for these two modes respectively. It is noted that as d is 12 nm, the higher-order mode and the dipole mode have equally contributed to Γ_{ii}. It is natural that the contribution of the higher order mode is suppressed by the dipole mode when $d = 12$ nm, which is shown in Fig. 2(b). In particular, when $d = 50$ nm, Γ_{ii} at the frequency of the ANP's dipole mode is ten times than that of the higher-order mode. The above result shows that the strength of Γ_{ii} is attributed mainly to the dipole mode when the QD is far from the surface of ANP. In addition, we find that the normalized spontaneous emission rate is less than five for $d > 50$ nm.

In contrast, the higher-order mode plays a dominant role and dramatically enhances the spontaneous emission rate when QD is close to the surface of ANP. Therefore, we set $d_a = 2$ nm and investigate the d_b-dependent Γ_{ij} and δ_{ij}. The other parameters are the same as those mentioned previously.

The influence of d_b on Γ_{ij} is shown in Figs. 3(a) and 3(b) for the small and large values of d_b, respectively. There exists three main peaks for Γ_{ij}, which are marked as P_1, P_2, and P_3, as shown in Figs. 3(a). It is clear that as d_b is increased, the Γ_{ij} decreases and shows a much stronger downtrend for the ANP's higher-order modes than for the dipole mode. For example, when d_b changes from 4 nm to 6 nm, Γ_{ij}/Γ_0 varies from 5.1×10^4 to 2.02×10^4 at the frequency of P_3, while Γ_{ij}/Γ_0 decreases from about 3600 to 2400. In addition, we find that Γ_{ij} has similar values at frequencies of P_1, P_2, and P_3 when $d_b = 22$ nm. Figure 3(b) shows a similar tendency of Γ_{ij}/Γ_0 to Fig. 3(a). We find that the influences of the higher-order modes of the ANP on Γ_{ij} can be ignored when $d_b > 120$ nm. Moreover, the dipole modes dominate Γ_{ij} when the QDs are far from the surface of the ANP.

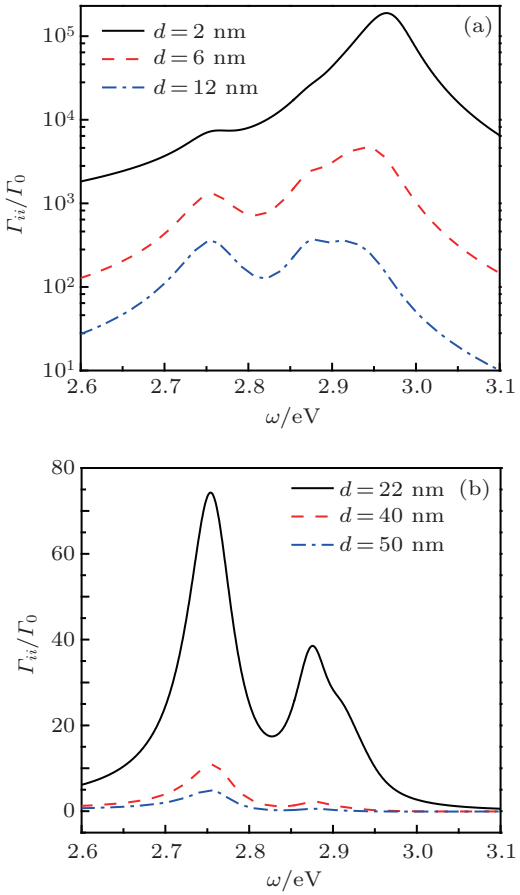


Fig. 2. (color online) Normalized spontaneous emission rate Γ_{ii}/Γ_0 versus frequency ω for the distance between the QDs and the surface of the ANP $d = 2$, 6, 12 nm (a), and 22, 40, 50 nm (b).

The potential energy of the DDI (δ_{ij}) is shown in Fig. 3(c). The dipole moments of the two dipoles are both set to be 24 D (1 D = 3.33564×10^{-30} C·m), which is comparable to the dipole moment used in other studies.[39] It is obvious that the numeric values of δ_{ij} are relatively small and δ_{ij} drops steeply as d_b increases. For instance, $\delta_{ij} \leq 8.817$ meV when d_b is 6 nm, $\delta_{ij} \leq 0.016$ meV as d_b is 90 nm, and $\delta_{ij} \leq 0.009$ meV while d_b is 140 nm. It is found that δ_{ij} is relatively small when $d_b = 22$ nm, which is beyond the scope of this work.

Figure 3(a) shows that the higher-order modes play the main role in RDDI for relatively small d_b. It becomes more and more weak as d_b is increased. We find that over a broad frequency range (the plateau region between P_2 and P_3) the Γ_{ij} nearly keeps constant for the case of $d_b = 22$ nm. In order to further investigate this phenomenon in depth, we change

the radius of the Ag nanosphere while the distances between the quantum dots and Ag nanosphere are fixed at $d_a = 2$ nm and $d_b = 22$ nm. The other parameters are the same as those mentioned previously. It is shown that an obvious plateau region is observed in Fig. 4 between P_2 and P_3. The frequency of P_2 is located at 2.878 eV, and the frequency of P_3 is located at 2.920 eV. It is noted that Γ_{ij} is nearly constant and the plateau region is very wide, above 0.05 eV. Although the radius of the Ag nanosphere is changed, the plateau region is nearly unchanged. This means that the radius of the Ag nanosphere has little effect on the plateau region when the quantum dots are fixed at a proper position. This plateau region may be useful for quantum entanglement, quantum information, biological detector, and other fields.

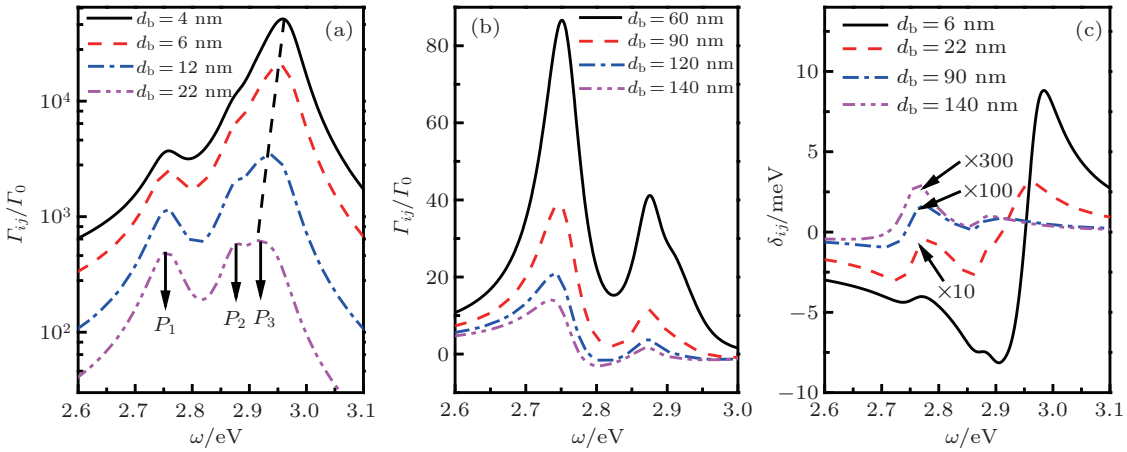


Fig. 3. (color online) The relationship between normalized Γ_{ij}/Γ_0 and ω for (a) $d_b = 4$, 6, 12, 22 nm, and (b) $d_b = 60$, 90, 120, 140 nm. (c) Variations of potential energy of the DDI (δ_{ij}) with ω for $d_b = 6$, 22, 90, and 140 nm. The values of d_a are all fixed to be 2 nm.

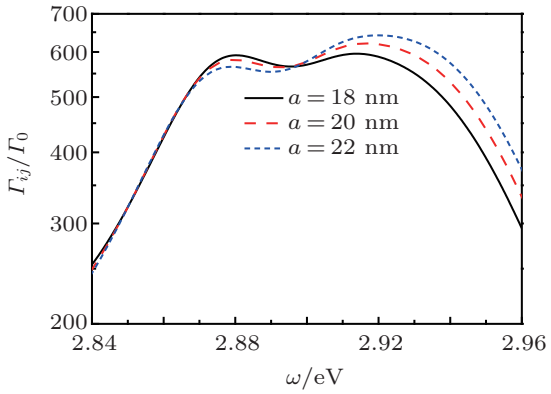


Fig. 4. (color online) Variations of normalized Γ_{ij}/Γ_0 with ω, with d_a and d_b fixed to be 2 nm and 22 nm, respectively, values of a being 18, 20, and 22 nm.

Figure 3(a) also shows another intriguing phenomenon where the peaks are red-shifted as d_b is increased. This phenomenon is similar to the case where the resonance peak of the extinction cross section of the ANP moves to a longer wavelength with the increase of its radius, where the dipole mode is modified by the higher-order modes under the long-wavelength approximation.[47] In this paper, we investigate the influence of the distance (d_b) on the frequency (ω_a), which corresponds to the maximum of Γ_{ij}. Here, d_a is fixed to be 2 nm, d_b is chosen to be from 4 nm to 100 nm and the other parameters are the same as those mentioned previously.

Figure 5(a) shows the influence of d_b on ω_a. The solid line, dashed line, and dot–dashed line indicate the relevant frequencies at P_1, P_2, and P_3, respectively, as shown in Fig. 3(a). It is clear that a monotonic decrease of ω_a is present as the one QD (d_b) is moved away while the other one and the ANP are fixed. The P_2 is inconspicuous for $d_b < 16$ nm in Fig. 3(a). In the inset of Fig. 5 (a_1), P_2 does not show an observable feature. While $d_b > 30$ nm, P_3 is difficult to observe, as indicated in the inset of Fig. 5 (a_3). It is shown that P_1, P_2, and P_3 can be seen clearly as d_b is between 16 nm and 30 nm in the inset of Fig. 5 (a_2) . We can see that each of the curves for P_1 and P_2 is nearly a horizontal line. However, the curve for the position of P_3 shifts dramatically compared with those of P_1 and P_2. To further explore the underlying physics behind this phenomenon, we examine the frequency shift at P_3 by changing the radius of the ANP. The results are shown in Fig. 5(b). Monotonic relationships between ω_a and d_b are found when the radii of the ANPs are 18, 20, and 22 nm. This shows that the radius has a slight influence on the monotonic relationship between ω_a and d_b. In addition, it is interesting that as d_b is increased by 2 nm, ω_a is reduced by about 5 meV, suggesting a tendency of the red-shift in wavelength.

In Fig. 6, we investigate the property of the transfer rate by fixing one QD and changing the locations of the other QD in plane. The x and y represent the coordinates of QD (B). Here, ω_1, ω_2, and ω_3 are the frequencies at P_1, P_2, and P_3, respectively, in Fig. 3(a). The values of ω are 2.75527 (ω_1), 2.87818 (ω_2), and 2.91964 (ω_3) eV, respectively, in Figs. 6(a) and 6(b), 6(c) and 6(d), and 6(e) and 6(f). For the large value of

d_a, the ANP dipole modes make the major contributions to Γ_{ij} in the left panels (6(a), 6(c), and 6(e)) when QDs are far from the ANP, even though the transition frequencies are different. However, as shown in the right panels, the dominant modes are related to the transition frequency. This phenomenon shows that the higher-order modes come into effect and may make a major contribution to Γ_{ij} if they match the transition frequency of the dipole as QDs are close to the ANP.

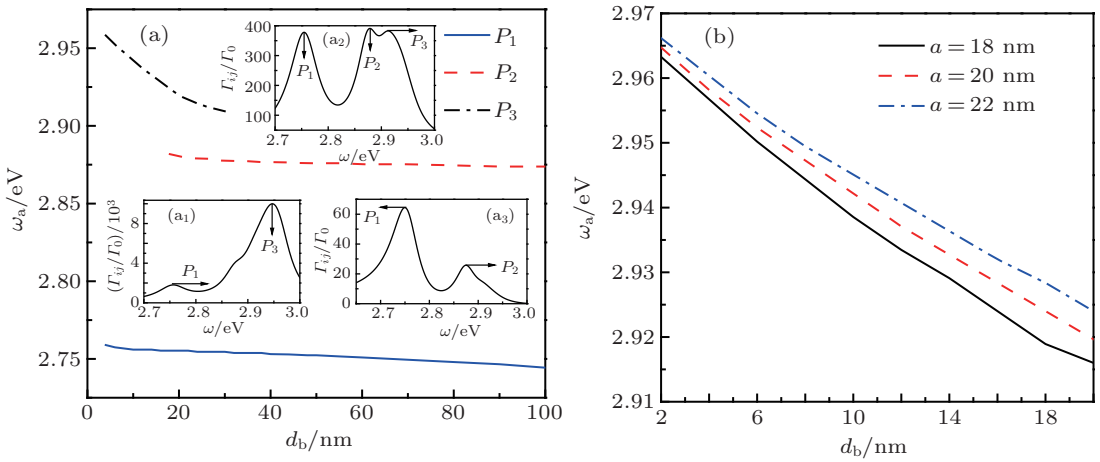


Fig. 5. (color online) Relationships between ω_a and d_b with the radius of the ANP $a = 18, 20, 22$ nm. Here ω_a corresponds to the maximum of Γ_{ij}/Γ_0, and d_a is fixed to 2 nm and d_b is changed.

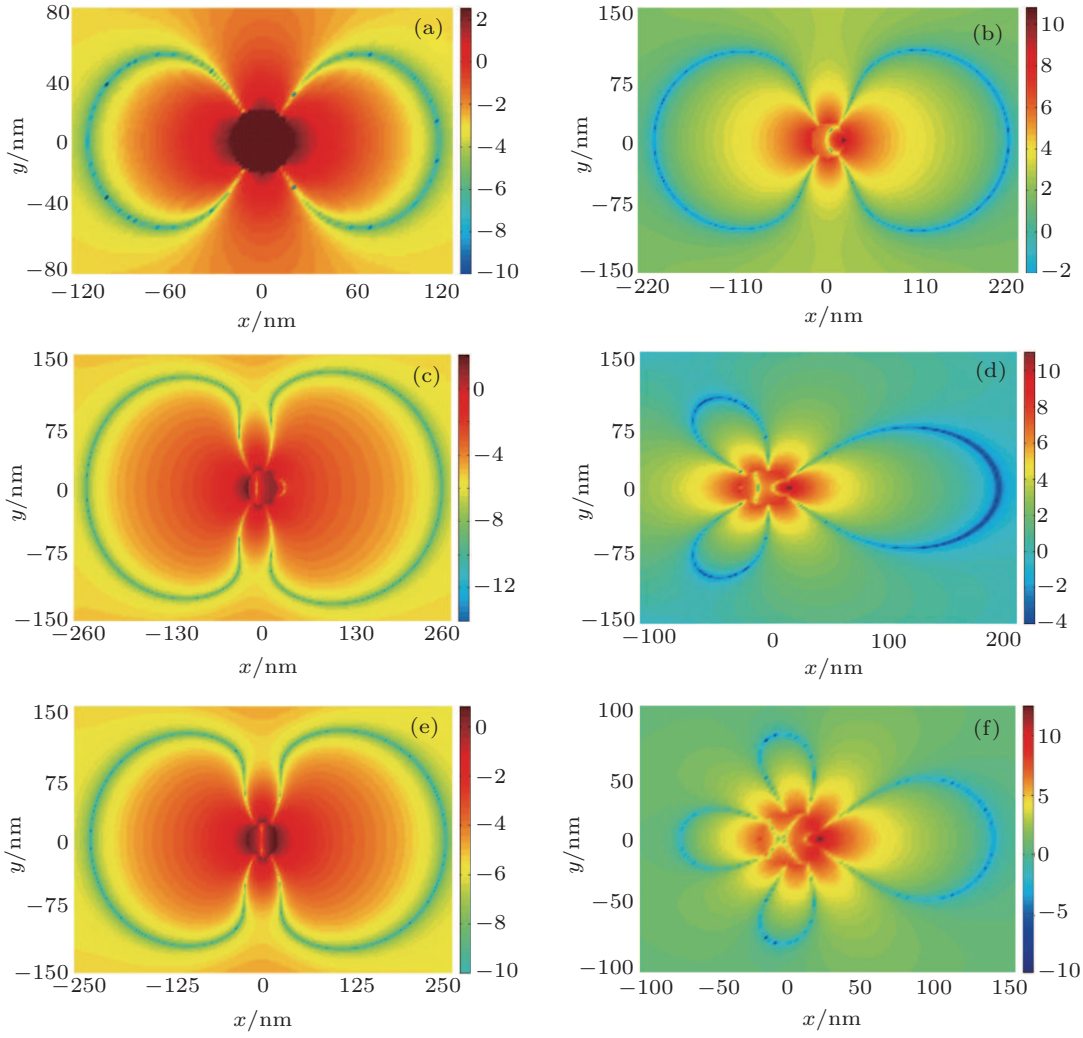


Fig. 6. (color online) The $\ln|\Gamma_{ij}/\Gamma_0|$ versus the position of atom B located at the xy plane. The $d_a = 140$ nm ((a), (c), and (e)) and 2 nm ((b), (d), and (f)), respectively, for different values of ω. The other parameters are the same as those mentioned previously.

4. Conclusion

In this paper, the analytical Green function approach is used to study the interaction between two QDs. The RDDI is systematically calculated while the QDs are placed at different positions, where one QD is fixed at 2 nm from the surface of the ANP and the other QD is moved in plane. Our results show that RDDI becomes weak as the distance between two QDs increases gradually. In addition, the influence of higher-order modes of the ANP on the RDDI declines more quickly than that of dipole modes. Γ_{ij} of the RDDI is nearly a constant over a broad frequency range where $d_{\rm b}$ is 22 nm and $d_{\rm a}$ is 2 nm, and the radius of ANP affects the above phenomenon slightly. The achievement of the wide frequency range can be useful in biology and medical sciences in the future. We find that the frequency corresponding to the maximum of Γ_{ij} has a monotonically decreasing relationship with the distance between the ANP and the QDs changing from 4 nm to 140 nm. In addition, the radius of ANP has little effect on it. We show that the dipole modes of ANP contribute mainly to Γ_{ij} when the distance is large. In contrast, when the distance is short, the higher-order modes of ANP become strong and dominate Γ_{ij} if they consist of a transition frequency of the dipole. It should be noted that our method is universally applicable and it can be extended to other systems including multiple ANPs and multiple QDs of different angles. Furthermore, the results can provide a theoretical basis for designing molecular biological detectors and gaining an insight into the artificial characteristics of microstructures and micro-devices in depth.

Appendix A

In the spherical coordinates, the scattering dyadic Green's functions are written in the following form:[44,45,47]

$$\begin{aligned}&\bar{G}^{\rm scatt}(r>a,r_{\rm o}>a;\omega)\\&=k_0^2\frac{-{\rm i}k_2}{4\pi}\sum_{\rm e,o}\sum_{n=1}^{\infty}\sum_{m=0}^{n}(2-\delta_m^0)\frac{2n+1}{n(n+1)}\frac{(n-m)!}{(n+m)!}\\&\quad\times[R_{\rm F}^{\rm H}M_{mn}^{\rm eo}(k_2r)M_{mn}^{\rm eo}(k_2r_{\rm o})+R_{\rm F}^{\rm V}N_{mn}^{\rm eo}(k_{\rm b}r)N_{mn}^{\rm eo}(k_2r_{\rm o})],\end{aligned}\tag{A1}$$

$$\begin{aligned}&\bar{G}^{\rm scatt}(r<a,r_{\rm o}>a;\omega)\\&=k_0^2\frac{-{\rm i}k_1}{4\pi}\sum_{n=1}^{\infty}\sum_{m=0}^{n}(2-\delta_m^0)\frac{2n+1}{n(n+1)}\frac{(n-m)!}{(n+m)!}\\&\quad\times[D_MM_{mn}(k_2)M_{mn}'^{(1)}(k_1)+D_NN_{mn}(k_2)M_{mn}'^{(1)}(k_1)],\end{aligned}\tag{A2}$$

where k_1 and k_2 are the wave vectors outside and inside the sphere, $R_{\rm F}^{\rm H}$ and $R_{\rm F}^{\rm V}$ are the centrifugal reflection coefficients corresponding to transverse electric (TE) wave and transverse magnetic (TM) wave, respectively, $M_{mn}^{\rm eo}$ and $N_{mn}^{\rm eo}$ are the vector functions corresponding to TE and TM waves and can be separated into even and odd contributions. The superscript (1) in $M_{mn}'^{(1)}$ denotes that the third-type spherical Bessel function or the first-type spherical Hanker function $\mathrm{h}_n^{(1)}(\rho)$, e (o) refers to even (odd).

The values of $R_{\rm F}^{\rm H}$, $R_{\rm F}^{\rm V}$, $R_{\rm P}^{\rm V}$, $T_{\rm F}^{\rm H}$, $T_{\rm P}^{\rm V}$, and $T_{\rm F}^{\rm V}$ are defined as follows:

$$R_{\rm P}^{\rm H}=\frac{\mu_1k_2\partial\kappa_2\kappa_1-\mu_2k_1\partial\kappa_1\kappa_2}{\mu_1k_2\tau_1\partial\kappa_2-\mu_2k_1\partial\tau_1\kappa_2},$$

$$R_{\rm F}^{\rm H}=\frac{\mu_1k_2\partial\tau_2\tau_1-\mu_2k_1\partial\tau_1\tau_2}{\mu_1k_2\partial\tau_2\kappa_1-\mu_2k_1\tau_2\partial\kappa_1},\tag{A3}$$

$$R_{\rm P}^{\rm V}=\frac{\mu_1k_2\kappa_2\partial\kappa_1-\mu_2k_1\kappa_1\partial\kappa_2}{\mu_1k_2\partial\tau_1\kappa_2-\mu_2k_1\tau_1\partial\kappa_2},$$

$$R_{\rm F}^{\rm V}=\frac{\mu_1k_2\tau_2\partial\tau_1-\mu_2k_1\tau_1\partial\tau_2}{\mu_1k_2\tau_2\partial\kappa_1-\mu_2k_1\partial\tau_2\kappa_1},\tag{A4}$$

$$T_{\rm P}^{\rm H}=\frac{\mu_1k_2(\tau_2\partial\kappa_2-\partial\tau_2k_2)}{\mu_1k_2\tau_1\partial\kappa_2-\mu_2k_1\partial\tau_1\kappa_2},$$

$$T_{\rm F}^{\rm H}=\frac{\mu_1k_2(\partial\tau_2\kappa_2-\tau_2\partial\kappa_2)}{\mu_1k_2\partial\tau_2\kappa_1-\mu_2k_1\tau_2\partial\kappa_1},\tag{A5}$$

$$T_{\rm P}^{\rm V}=\frac{\mu_1k_2(\partial\tau_2\kappa_2-\tau_2\partial\kappa_2)}{\mu_1k_2\partial\tau_1\kappa_2-\mu_2k_1\tau_1\partial\kappa_2},$$

$$T_{\rm F}^{\rm V}=\frac{\mu_1k_2(\tau_2\partial\kappa_2-\partial\tau_2\kappa_2)}{\mu_1k_2\tau_2\partial\kappa_1-\mu_2k_1\partial\tau_2\kappa_1},\tag{A6}$$

$$D_{M,N}=\frac{-1}{T_{\rm P}^{\rm H,V}}[R_{\rm F}^{\rm H,V}R_{\rm P}^{\rm H,V}-1],\tag{A7}$$

$$\tau_{\rm i}=\mathrm{J}_n(k_ia),\quad \kappa_i=\mathrm{h}_n^{(1)}(k_ia),\tag{A8}$$

$$\partial\tau_i=\frac{1}{k_ia}\frac{\partial[k_ia\,\mathrm{j}_n(k_ia)]}{\partial k_ia},\quad \partial\kappa_i=\frac{1}{k_ia}\frac{\partial[k_ia\,\mathrm{h}_n^{(1)}(k_ia)]}{\partial k_ia},\tag{A9}$$

where the subscripts F and P denote the centrifugal and centripetal waves, respectively, $T_{\rm (P,F)}^{\rm H}$ and $R_{\rm (P,F)}^{\rm H}$ represent the centripetal and centrifugal transmission and reflection contributions from TE waves (corresponding to the superscript H), while $T_{\rm (P,F)}^{\rm V}$ and $R_{\rm (P,F)}^{\rm V}$ represent the centripetal and centrifugal transmission and reflection contributions from TM waves (corresponding to the superscript V), $\mathrm{J}_n(\rho)$ is the first-type spherical Bessel function, k_i equals $\omega\sqrt{\varepsilon_i}/x$, i.e., $k_i=\omega\sqrt{\varepsilon_i}/x$, with i corresponding to the metal or background.

The vector functions are defined as follows:[46]

$$\begin{aligned}M_{mn}^{\rm e}(kr)=&-\frac{m}{\sin\theta}\mathrm{h}^{(1)}(kr)\mathrm{P}_n^m(\cos\theta)\sin m\phi\,\widehat{\theta}\\&-\mathrm{h}^{(1)}(kr)\frac{\mathrm{d}\mathrm{P}_n^m(\cos\theta)}{\mathrm{d}\theta}\cos m\phi\,\widehat{\phi},\end{aligned}\tag{A10}$$

$$\begin{aligned}M_{mn}^{\rm o}(kr)=&\frac{m}{\sin\theta}\mathrm{h}^{(1)}(kr)\mathrm{P}_n^m(\cos\theta)\cos m\phi\,\widehat{\theta}\\&-\mathrm{h}^{(1)}(kr)\frac{\mathrm{d}\mathrm{P}_n^m(\cos\theta)}{\mathrm{d}\theta}\sin m\phi\,\widehat{\phi},\end{aligned}\tag{A11}$$

$$\begin{aligned}N_{mn}^{\rm e}(kr)=&\frac{n(n+1)}{kr}\mathrm{h}^{(1)}(kr)\mathrm{P}_n^m(\cos\theta)\cos m\phi\,\widehat{r}\\&+\frac{1}{kr}\frac{\mathrm{d}[r\mathrm{h}^{(1)}(kr)]}{\mathrm{d}r}\left[\frac{\mathrm{d}\mathrm{P}_n^m(\cos\theta)}{\mathrm{d}\theta}\cos m\phi\,\widehat{\theta}\right.\\&\left.-\frac{m}{\sin\theta}\mathrm{P}_n^m(\cos\theta)\cos m\phi\,\widehat{\phi}\right],\end{aligned}\tag{A12}$$

$$N_{mn}^{\rm o}(kr)=\frac{n(n+1)}{kr}\mathrm{h}^{(1)}(kr)\mathrm{P}_n^m(\cos\theta)\sin m\phi\,\widehat{r}$$

$$+\frac{1}{kr}\frac{\mathrm{d}[r\mathrm{h}^{(1)}(kr)]}{\mathrm{d}r}\left[\frac{\mathrm{d}\mathrm{P}_n^m(\cos\theta)}{\mathrm{d}\theta}\sin m\phi\,\widehat{\theta}\right.$$
$$\left.+\frac{m}{\sin\theta}\mathrm{P}_n^m(\cos\theta)\cos m\phi\,\widehat{\phi}\right], \quad \text{(A13)}$$

where P_n^m is the associated Legendre function of first kind with order (n, m). In order to simplify numerical calculation, we consider the condition in the x–y plane ($z = 0$), i.e., $\theta = \pi/2$.

References

[1] Purcell E M 1946 *Phys. Rev.* **69** 681
[2] Yokoyama H 1992 *Science* **256** 66
[3] Wang Y, Wu Q, He X J, Zhang S Q and Zhung L L 2009 *Chin. Phys. B* **18** 1801
[4] Liu S P, Li J H, Yu R and Wu Y 2013 *Phys. Rev. A* **87** 042306
[5] Thon S M, Rakher M T, Kim H, Gudat J, Irvine W T M, Petroff P M and Bouwmeester D 2009 *Appl. Phys. Lett.* **94** 111115
[6] Wang X H, Gu B Y, Wang R Z and Xu H Q 2003 *Phys. Rev. Lett.* **91** 113904
[7] Liu Z Q, Feng T H, Dai Q F, Wu L J, Lan S, Ding C R, Wang H Z and Venu G A 2010 *Chin. Phys. B* **19** 114210
[8] Agarwal G S 1975 *Phys. Rev. A* **12** 1475
[9] Meschede D, Walther H and Muller G 1985 *Phys. Rev. Lett.* **54** 551
[10] Guo H and Xiong H N 2008 *Chin. Phys. B* **17** 971
[11] Lu H Y, Lu H, Zhang J N, Qiu R Z, Pu H and Yi S 2010 *Phys. Rev. A* **82** 023622
[12] Cheng M T, Ma X S and Wang X 2014 *Chin. Phys. Lett.* **31** 014202
[13] Kim H, Sridharan D, Shen T C, Solomon G S and Waks E 2011 *Opt. Express* **19** 2589
[14] Zhou F, Liu Y and Li Z Y 2011 *Opt. Lett.* **36** 1969
[15] Martín-Cano D, González-Tudela A, Martín-Moreno L, García-Vidal F J, Tejedor C and Moreno E 2011 *Phys. Rev. B* **84** 235306
[16] Yang P F, Di Z G and Xu H X 2013 *Opt. Express* **21** 17053
[17] Dai D X and He S L 2010 *Opt. Express* **18** 17958
[18] Berini P 2000 *Phys. Rev. B* **61** 10484
[19] Takahara J, Yamagishi S, Taki H, Morimoto A and Kobayashi T 1997 *Opt. Lett.* **22** 475
[20] Pile D F P, Ogawa T, Gramotnev D K, Matsuzaki Y, Vernon K C, Yamaguchi K, Okamoto T, Haraguchi M and Fukui M 2005 *Appl. Phys. Lett.* **87** 261114
[21] Tong L M and Xu H X 2012 *Physics* **41** 582 (in Chinese)
[22] Yao P and Hughes S 2009 *Opt. Express* **17** 11505
[23] Liu S P, Yu R, Li J H and Wu Y 2013 *J. Appl. Phys.* **114** 244306
[24] Hughes S 2005 *Phys. Rev. Lett.* **94** 227402
[25] Huang Y G, Chen G Y, Jin C J, Liu W M and Wang X H 2012 *Phys. Rev. A* **85** 053827
[26] Liao X P, Fang M F, Cai J W and Zheng X J 2008 *Chin. Phys. B* **17** 2137
[27] Cui L K, Zhang Y J, Man Z X and Xia Y J 2012 *Chin. Phys. B* **21** 100202
[28] Chen L Shao X Q and Zhang S 2009 *Chin. Phys. B* **18** 0888
[29] Ruostekoski J and Javanainen J 1997 *Phys. Rev. A* **55** 513
[30] Xie H Y, Chung H Y, Leung P T and Tsai D P 2009 *Phys. Rev. B* **80** 155448
[31] Dung H T, Knöll L and Welsch D G 2002 *Phys. Rev. A* **66** 063810
[32] Protsenko I E, Uskov A V, Zaimidoroga O A, Samoilov V N and O'Reilly E P 2005 *Phys. Rev. A* **71** 063812
[33] Reinhard A, Younge K C, Liebisch T C, Knuffman B, Berman P R and Raithel G 2008 *Phys. Rev. Lett.* **100** 233201
[34] Saquet N, Cournol A, Beugnon J, Robert J, Pillet P and Vanhaecke N 2010 *Phys. Rev. Lett.* **104** 133003
[35] Harlander M, Lechner R, Brownnutt M, Blatt R and Ha Sel W 2011 *Nature* **471** 200
[36] Agarwal G S and DuttaGupta S 1998 *Phys. Rev. A* **57** 667
[37] Gonzalez-Tudela A, Martin-Cano D, Moreno E, Martin-Moreno L, Tejedor C and Garcia-Vidal F J 2011 *Phys. Rev. Lett.* **106** 020501
[38] Schmid S I and Evers J 2008 *Phys. Rev. A* **77** 013822
[39] Agarwal G S and Patnaik A K 2001 *Phys. Rev. A* **63** 043805
[40] Goldstein E V and Meystre P 1997 *Phys. Rev. A* **56** 5135
[41] Kobayashi T, Zheng Q B and Sekiguchi T 1995 *Phys. Rev. A* **52** 2835
[42] Rist S, Eschner J, Hennrich M and Morigi G 2008 *Phys. Rev. A* **78** 013808
[43] Bay S, Lambropoulos P and Mølmer K 1997 *Phys. Rev. A* **55** 1485
[44] Novotny L and Hecht B 2006 *Principles of Nano-Optics*, Vol. 1 (Cambridge: Cambridge University Press) pp. 260–298
[45] Tai C T 1971 in *Dyadic Green's Functions in Electromagnetic Theory* (Scranton: Intext Educational Publishers) pp. 55–66
[46] Vlack C V, Kristensen P T and Hughes S 2012 *Phys. Rev. B* **85** 075303
[47] Li L W, Kooi P S, Leong M S and Yeo T S 1994 *IEEE Trans. Microwave Theor. Tech.* **42** 2302
[48] Jensen T, Kelly L, Lazarides A and Schatz G C 1999 *J. Clust. Sci.* **10** 295